EFFECT OF Ag NANOPARTICLE SHAPE ON CIGS SOLAR CELL EFFICIENCY

Khaitbaev Eldorbek
Urgench State university named after Abu Rayhan Biruni Institute, Urgench, Uzbekistan;
Department of Physics and Astronomy, Urgench state pedagogical institute
eldorkhaitbaev@urdu.uz
Jumaboev Bekhzod
Atamuratov Atabek
Urgench State university named after Abu Rayhan Biruni Institute, Urgench, Uzbekistan
https://doi.org/10.5281/zenodo.24041444

Abstract. At equal surface coverage, the shape of Ag nanoparticles embedded in the CdS buffer decides whether they raise or lower the efficiency of a CIGS solar cell. We modelled a Mo/CIGS (1000 nm)/CdS (70 nm)/i-ZnO (50 nm)/ZnO:(H,Al) (250 nm) cell with coupled 3D FDTD optical and CHARGE drift-diffusion simulations in ANSYS Lumerical 2020 R2.4. Two Ag particles per 187.5 nm periodic cell gave a projected coverage of 16.08 % for spheres (r = 30 nm), upright cylinders (r = 30 nm, h = 60 nm) and cubes (a = 53.17 nm), all resting on the CIGS surface. Spheres raised the power conversion efficiency from 16.65 % to 16.89 % (+0.23 % abs.), mainly through a higher short-circuit current density (32.14 vs 31.67 mA/cm²). Cylinders and cubes lowered it to 14.91 % and 15.61 %, as J_{sc} fell to 28.24 and 29.59 mA/cm². Optical generation in CIGS dropped from 24.80 mA/cm² (no particles) to 22.00 and 21.40 mA/cm², and parasitic absorption in Ag doubled relative to spheres. We attribute the loss to shading of the absorber by the flat particle bases in direct contact with CIGS, and to the larger metal volume. For plasmonic light management in CIGS, the particle–absorber contact geometry matters as much as the projected coverage.

Keywords: CIGS; plasmonic nanoparticles; silver; particle shape; FDTD; CHARGE; thin-film solar cells; light trapping

1. Introduction

$Cu(In,Ga)Se_2$ (CIGS) thin-film solar cells have reached laboratory efficiencies of 22.6 % [1], and thinning the absorber to save indium and gallium makes light management increasingly important. Metal nanoparticles that support localized surface plasmons can scatter light into the absorber and concentrate the near field around themselves, raising absorption in thin layers [2]. Ag particles on silicon cells enhanced absorption by up to sixteenfold near the band gap of a 1.25 µm layer [3].

The benefit depends strongly on particle shape and on how the particle couples to the substrate. Catchpole and Polman showed that cylinders and hemispheres on a high-index substrate give much larger path-length enhancement than spheres, because of stronger near-field coupling [4]. On the front side of a cell, however, the same coupling can raise absorption in the metal and reflection through Fano-type interference [5]. The net effect of shape therefore has to be judged at the level of the whole device, from optics to collected current.

Most CIGS plasmonic studies compare particle size or coverage for spheres. A direct shape comparison at equal projected coverage, carried through to the J–V characteristics, is still missing. In

earlier work with the same calibrated model, Ag spheres embedded in the CdS buffer raised the efficiency of a 1000 nm CIGS cell at 16.08 % coverage.

This study asks whether that gain survives a change of shape. We compare spheres, upright cylinders and cubes of equal projected area, placed in the CdS buffer on the CIGS surface. We report the optical spectra, the generation profiles and the electrical parameters for each shape against a particle-free reference.

2. Methods

2.1 Device structure

The cell is a substrate-configuration stack: Mo (900 nm) / CIGS (1000 nm, GGI = 0.5) / CdS (70 nm) / i-ZnO (50 nm) / ZnO:(H,Al) (250 nm). Layer optical constants and electrical parameters follow a model previously calibrated against a published reference cell. The calibrated model uses an SRH lifetime of 2.3 ns in CIGS, an acceptor density of 5×10^{15} cm^{-3}, a series resistance of 2.25 Ω cm² and a shunt resistance of 1000 Ω cm².

2.2 Nanoparticle geometries

Each square periodic cell (P = 187.5 nm) holds two Ag particles on its diagonal at (−P/4, −P/4) and (+P/4, +P/4) from the cell centre. All particles sit inside the CdS buffer with their lowest point on the CIGS surface. Shapes were sized to the same projected area, so the coverage $S/S_0 = 2A/P^2$ is 16.08 % in every case.

Table 1. Ag particle geometries at equal projected coverage (16.08 %).

Shape	Dimensions	Projected area A (nm²)	Volume per particle (nm³)	Contact with CIGS
Sphere	r = 30 nm	2827	113 097	point
Cylinder (axis ∥ z)	r = 30 nm, h = 60 nm	2827	169 646	flat base, 2827 nm²
Cube	a = r√π = 53.17 nm	2827	150 345	flat base, 2827 nm²

Ag optical constants were taken from Johnson and Christy [6]. A particle-free cell of the same period served as the reference.

2.3 Optical simulation (FDTD)

Optical fields were computed with 3D FDTD (ANSYS Lumerical FDTD 2020 R2.4). A normally incident plane-wave source spanned 300–1200 nm with 61 frequency points. Periodic boundaries were used in x and y and PML in z. The mesh was auto non-uniform (accuracy 2), refined to 1.25 nm in all directions across the CdS layer and to 2.5 nm in z from 850 nm to the top of the stack. Runs stopped at an auto-shutoff level of 10^{-5}.

Layer absorption was obtained from power-flux monitors at each interface. Absorption in the Ag particles was integrated from a 3D field monitor over the CdS layer as $\tfrac{1}{2}\omega\varepsilon_0\,\mathrm{Im}(\varepsilon_{Ag})|E|^2$ within the particle volume, and subtracted from the CdS flux balance. Generation rates in CIGS, CdS and i-ZnO were obtained under AM1.5G with solar-generation analysis groups; Ag mesh points were set to zero.

2.4 Electrical simulation (CHARGE)

The 3D generation profiles were averaged along y and imported into a 2D CHARGE drift-diffusion model of the same stack. A generation scale factor of 1.26 from the calibration was applied to all cases. A

voltage sweep from 0 to 0.74 V in 20 mV steps gave the J–V curve, from which J_{sc}, V_{oc}, FF and PCE were extracted under 100 mW/cm².

The sphere case was taken from our earlier run with the identical model and scripts. The reference, cylinder and cube cases were computed for this study.

3. Results

3.1 Photovoltaic performance

Only the spheres improved the cell: PCE rose by 0.23 % abs., while cylinders and cubes lost 1.75 and 1.05 % abs. (Table 2). The change comes almost entirely from J_{sc}; V_{oc} moved by less than 5 mV and FF by less than 0.7 % abs. The small FF gain of the cylinder and cube cells follows from their lower current through the series resistance.

Table 2. Photovoltaic parameters under AM1.5G (100 mW/cm²), coverage 16.08 %.

Cell	J_{sc} (mA/cm²)	V_{oc} (mV)	FF (%)	PCE (%)	ΔPCE (% abs.)
No particles	31.67	747.7	70.34	16.65	—
Ag spheres	32.14	748.2	70.22	16.89	+0.23
Ag cylinders	28.24	743.4	71.00	14.91	−1.75
Ag cubes	29.59	745.2	70.79	15.61	−1.05

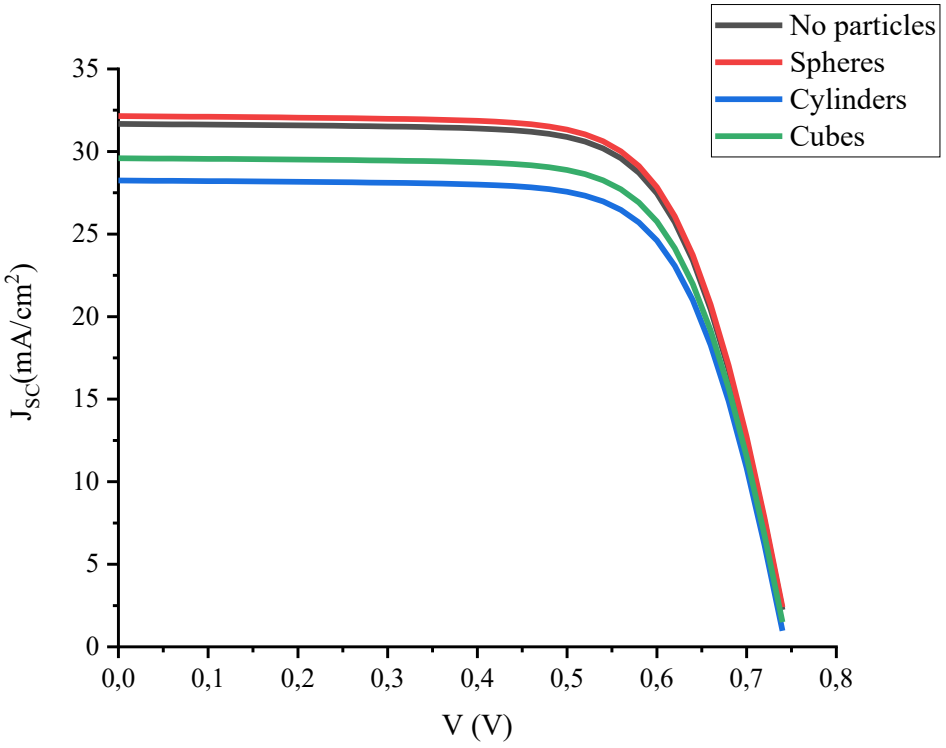


Figure 1. J–V characteristics of the four cells. The curves keep their shape and shift almost rigidly with J_{sc}, confirming that particle shape acts through photocurrent rather than through recombination.

3.2 Optical absorption

The shape changes where the light goes, not how much the stack absorbs in total. Averaged over 300–1200 nm, total absorption was 0.78 without particles and 0.79–0.81 with them. In the CIGS layer, however, all particles reduced absorption below 580 nm, and only spheres recovered it at longer wavelengths: in the 700–900 nm band they raised it from 0.775 to 0.804, whereas cylinders and cubes lowered it to 0.753 and

0.719 (Fig. 2). Between 500 and 700 nm the flat-based particles cut CIGS absorption from 0.647 to 0.52 and 0.51.

Table 3. Band-averaged absorption in CIGS (A_{CIGS}), in Ag (A_{Ag}) and reflectance (R).

Band (nm)	Quantity	No particles	Spheres	Cylinders	Cubes
300–500	A_{CIGS}	0.253	0.149	0.135	0.151
500–700	A_{CIGS}	0.647	0.619	0.522	0.505
700–900	A_{CIGS}	0.775	0.804	0.753	0.719
900–1200	A_{CIGS}	0.301	0.302	0.283	0.274
500–700	A_{Ag}	0	0.006	0.013	0.014
700–900	A_{Ag}	0	0.002	0.013	0.016
500–700	R	0.217	0.129	0.163	0.169
700–900	R	0.125	0.081	0.090	0.113

All particles reduced reflectance, most strongly the spheres. Parasitic absorption in Ag was two to eight times higher for cylinders and cubes than for spheres, depending on the band.

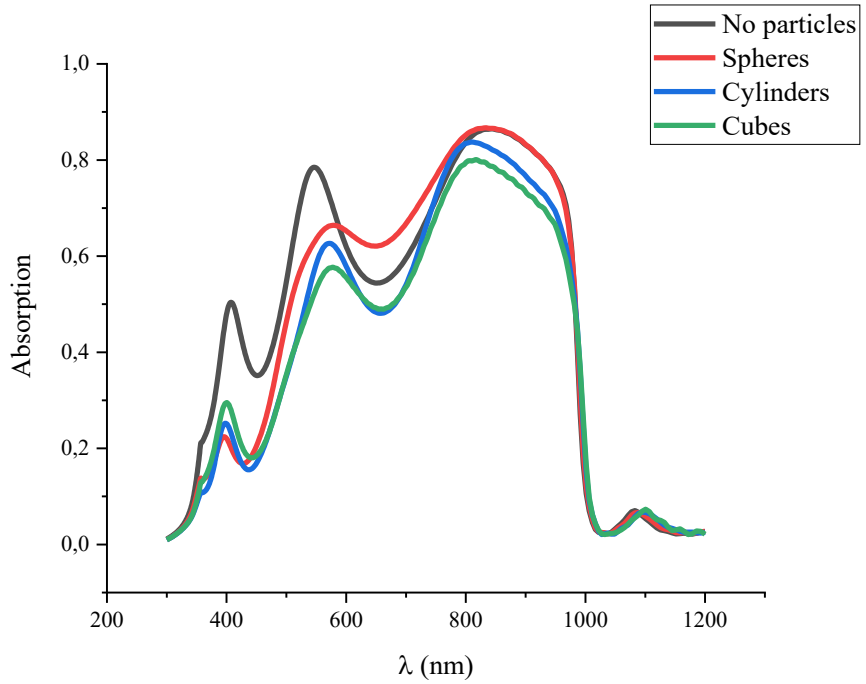


Figure 2. Absorption spectra of the CIGS layer. Every particle cell absorbs less in CIGS below 580 nm, where CdS absorption rises. The sphere cell exceeds the reference from 600 to 900 nm (shaded: 700–900 nm band of Table 3). Cylinders and cubes stay below it over most of 450–980 nm, where the AM1.5G photon flux is highest.

3.3 Generation

Integrated optical generation in CIGS fell from 24.80 mA/cm² without particles to 24.25 (spheres), 22.00 (cylinders) and 21.40 mA/cm² (cubes), before the calibration factor of 1.26. Generation in the CdS buffer rose from 3.90 to 6.49, 7.57 and 7.46 mA/cm². In all particle cells the generation peak moved towards the CIGS/CdS interface: at z = 1897.5 nm it reached 1.3×10^{28} m^{-3} s^{-1} for spheres, against 4.5×10^{28} and 5.2×10^{28} for cylinders and cubes. Because the buffer is n-type CdS within the junction, carriers

generated there still contribute to the current in the model, which is why the sphere cell gains J_{sc} even though its CIGS generation is slightly lower than the reference.

4. Discussion

The flat-based particles lose current because they shade the absorber they touch. A sphere meets the CIGS at a single point, so light can reach the absorber around and beneath it, and its forward scattering couples into CIGS over the whole footprint. A cylinder or cube covers 16 % of the CIGS surface with an opaque metal face in direct contact. The loss of CIGS absorption at 500–700 nm (about 0.13–0.14) is close to that 16 % geometric shadow, which supports this reading.

The flat-based shapes also absorb more light in the metal. Their contact face sits in the strongest near field of the high-index CIGS, and they hold 33–50 % more silver than a sphere of the same footprint. Both raise ohmic loss, seen as the higher A_{Ag} in Table 3. This agrees with the finding that near-field coupling to the substrate shifts and broadens plasmon resonances [4,5]. In our front-side geometry, the extra coupling feeds loss rather than useful scattering.

These results look opposite to the well-known advantage of cylinders and hemispheres [4]. The two are consistent once the geometry is considered. That advantage was found for path-length enhancement in a substrate below the particle, where the near field and scattering go into the absorber. Here the particles sit in a 70 nm buffer on top of the absorber, with the incident light arriving from above, so the same near field draws energy into the metal and the base blocks direct transmission.

The cube cell gave 1.35 mA/cm² more J_{sc} than the cylinder cell, although its integrated generation was slightly lower (21.40 + 7.46 vs 22.00 + 7.57 mA/cm² in CIGS + CdS). A likely cause is the spatial distribution: the cube concentrates more generation in the last few nanometres of CIGS below the junction, where collection is most efficient. The present data do not settle this, and the difference is small next to the gap between point-contact and flat-contact shapes.

The study has limits. Particles are perfectly regular, aligned with the field and free of oxide shells. Carriers generated in CdS are fully collected in the drift-diffusion model, which likely overstates the sphere gain. The sphere case comes from an earlier run of the same model rather than from the present batch. Only one coverage, one particle size and normal incidence were simulated.

For design, the results point to particles that keep a small contact area with the absorber: spheres, or flat shapes lifted by a dielectric spacer of a few nanometres. Testing cylinders and cubes on a 5–10 nm spacer would separate the shading effect from the shape effect.

5. Conclusion

At the same 16.08 % projected coverage, Ag spheres in the CdS buffer raised the efficiency of a 1000 nm CIGS cell from 16.65 % to 16.89 %, while cylinders and cubes lowered it to 14.91 % and 15.61 %. The loss stems from shading of the absorber by flat particle bases in direct contact with CIGS and from higher parasitic absorption in the larger metal volume. Projected coverage alone does not fix the plasmonic effect; the contact geometry between particle and absorber must be designed as well. Spheres, or flat particles separated from CIGS by a thin spacer, are the preferred choice for front-side plasmonic CIGS cells.

References

1. P. Jackson, R. Wuerz, D. Hariskos, E. Lotter, W. Witte, M. Powalla, "Effects of heavy alkali elements in Cu(In,Ga)Se_2 solar cells with efficiencies up to 22.6 %," Phys. Status Solidi RRL **10**, 583–586 (2016). doi:10.1002/pssr.201600199.
2. H. A. Atwater, A. Polman, "Plasmonics for improved photovoltaic devices," Nat. Mater. **9**, 205–213 (2010). doi:10.1038/nmat2629.
3. S. Pillai, K. R. Catchpole, T. Trupke, M. A. Green, "Surface plasmon enhanced silicon solar cells," J. Appl. Phys. **101**, 093105 (2007). doi:10.1063/1.2734885.
4. K. R. Catchpole, A. Polman, "Design principles for particle plasmon enhanced solar cells," Appl. Phys. Lett. **93**, 191113 (2008). doi:10.1063/1.3021072.
5. P. Spinelli, M. Hebbink, R. de Waele, L. Black, F. Lenzmann, A. Polman, "Optical impedance matching using coupled plasmonic nanoparticle arrays," Nano Lett. **11**, 1760–1765 (2011). doi:10.1021/nl200321u.
6. P. B. Johnson, R. W. Christy, "Optical constants of the noble metals," Phys. Rev. B **6**, 4370 (1972). doi:10.1103/PhysRevB.6.4370.